

## Article

# Enhanced Crashworthiness Parameters of Nested Thin-Walled Carbon Fiber-Reinforced Polymer and Al Structures: Effect of Using Expanded Polypropylene Foam

Muhammet Muaz Yalçın \*  and Mehmet İskender Özsoy

Department of Mechanical Engineering, Sakarya University, Sakarya 54050, Turkey; iozsoy@sakarya.edu.tr

\* Correspondence: myalcin@sakarya.edu.tr; Tel.: +90-264-2955858

**Abstract:** The in-plane loading conditions of carbon fiber/epoxy composite (CFRP) and aluminum nested-tube-reinforced expanded polypropylene (EPP) blocks were empirically examined. This study used crashworthiness metrics to estimate the best design configuration under quasi-static loading rates. The experimental phase began with lateral loading testing of single and nested aluminum and CFRP specimen. In-plane crushing experiments were performed on EPP foam blocks reinforced with nested tubes. Both single and nested aluminum tubes had comparable force–response curves and maintained their load-bearing capacity throughout testing. Despite a load-carrying capacity drop above a particular displacement threshold, the CFRP specimens had superior specific energy absorption (SEA) values due to their lightweight nature. The triple-tube nested specimens with two smaller tubes exhibited the best SEA results (1.72 and 1.88 J/g, respectively, for the aluminum and CFRP nested samples). During concurrent tube deformation, the nested samples showed a synergistic connection that increased energy absorption, especially in the EPP foam blocks with reinforced tubes. The study also examined the effects of building nested specimens with aluminum exterior tubes and CFRP inner tubes, and vice versa. This method showed that CFRP tubes within aluminum outer tubes lowered specimen weight (from 93.1 g to 67.7 g) and energy absorption (from 160.2 J to 153.3 J). However, the weight reduction outweighed the energy absorption, increasing SEA values for certain composite material configurations (from 1.72 J/g to 2.26 J/g).



**Citation:** Yalçın, M.M.; Özsoy, M.İ. Enhanced Crashworthiness Parameters of Nested Thin-Walled Carbon Fiber-Reinforced Polymer and Al Structures: Effect of Using Expanded Polypropylene Foam. *Appl. Sci.* **2024**, *14*, 9635. <https://doi.org/10.3390/app14219635>

Academic Editor: Ana Martins Amaro

Received: 14 August 2024

Revised: 3 October 2024

Accepted: 18 October 2024

Published: 22 October 2024



**Copyright:** © 2024 by the authors. Licensee MDPI, Basel, Switzerland. This article is an open access article distributed under the terms and conditions of the Creative Commons Attribution (CC BY) license (<https://creativecommons.org/licenses/by/4.0/>).

**Keywords:** crashworthiness; CFRP; nested tubular structures; EPP foam; in-plane loading; lateral crushing

## 1. Introduction

Energy absorbers represent a critical aspect of passive safety mechanisms within vehicular systems, functioning to mitigate the impact force during collisions. Their primary objective is to minimize vehicular damage and, by extension, enhance occupant protection [1–3]. Within this context, thin-walled metallic structures emerge as pivotal components, particularly in the automotive and aerospace sectors. These structures are distinguished by their lightweight nature, cost-effectiveness, and superior energy absorption capabilities [4–6]. Predominantly, steel and aluminum are the materials of choice in these applications [7], owing to their optimal balance of strength and ductility. Moreover, the energy absorption process in metallic tube structures is achieved through plastic deformation, which effectively dissipates collision energy. This deformation is influenced by the direction of load application, whether axial or lateral [8,9], underscoring the importance of design considerations in the development of effective energy absorbers.

While examining the energy absorption characteristics of tubes under axial and lateral loads, it was observed that tubes with circular cross-sections exhibit superior energy absorption capabilities when subjected to axial loading as compared to lateral loading. However, this advantage is mitigated by the presence of significant fluctuations during

loading, the manifestation of global bending, and the emergence of unstable deformation modes when subjected to off-axis loading [10]. Conversely, when tubes are exposed to lateral loading, they are characterized by the absence of unstable deformations in off-axis scenarios, alongside the observation of large displacements and a force curve that delineates a more consistent trend. This discrepancy underscores the distinct mechanical behaviors inherent to loading directions and serves as a basis for the utilization of nested tubular structures as an efficacious strategy for augmenting the energy dissipation behavior of tubes, particularly in contexts where the stroke distance is constrained [11]. Nested tubes, typically incorporating circular or rectangular cross-sections, are configured by placing multiple tubes within each other, thus forming at least a dual-tube arrangement [12]. The application of nested tubes as energy absorbing components culminates in enhanced performance against lateral loads, primarily attributed to the expansion of plastic deformation zones facilitated by the constraining effect of the nested configuration [13].

This paper delves into the exploration of various determinants influencing the energy absorption capabilities of nested metal tubes when subjected to both quasi-static and dynamic loading conditions. Specifically, the research elucidates the impact of material composition, tube diameter, wall thickness, and the spatial arrangement of these tubes on their capacity to mitigate energy [14–17]. Steel, owing to its commendable strength, ductility, and exceptional collision energy absorption properties, is predominantly employed within the automotive sector [18–20]. The investigation conducted by Shabani et al. [21] casts light on how the wall thickness and the strategic arrangement of single and nested steel tubes, varying in diameter, under lateral impact loading, culminate in a markedly enhanced energy dissipation efficacy in nested-tube configurations. Furthermore, research by Olabi et al. [22] into the lateral crushing behavior of nested steel tubes under impact tests, and Baroutaji et al.'s [23] experimental and parametric analysis using a finite element methodology on the array of behaviors of nested steel tubes underscore the superior energy absorption capacity facilitated by specific arrangements and dimensional characteristics of these tubes. Additionally, Kahraman and Akdikmen's study [24] on the lateral crushing behavior of nested steel tubes presents a comparative analysis based on diameters, combinations, and uniform wall thicknesses under compression tests. In parallel, the application of aluminum alloys is extensively recognized in the automotive and aerospace industries, and is attributed to their high specific strength, ductility, corrosion resistance, and cost-effectiveness [25,26]. Research by Xu et al. [11] on the lateral deformation behaviors under quasi-static and impact loading of nested-tube systems employing aluminum and steel elucidates the significant effects of material choice and tube combination on deformation behavior. Lastly, Wu et al.'s study [27] on the deformation behavior of nested structures comprising elliptical tubes within corrugated tubes under lateral compression tests highlights the critical interaction between the corrugation and the internal tube, significantly impacting the energy dissipation behavior. This comprehensive body of research significantly contributes to the ongoing advancements in the field of materials science, particularly in the optimization of the energy absorption capacities of nested-tube structures for enhanced safety and efficiency in automotive and aerospace applications.

Nested tubular configurations have been increasingly recognized for their potential as energy dissipation mechanisms in the face of impacts and explosive forces. In the realm of material science and engineering, Wang et al. [12] investigated the incorporation of steel triangular structures within circular tubes as a method to counteract the effects of impact and explosion energies. Their research primarily focused on examining how variations in the circular tube's thickness, along with the geometric alterations in the triangular shape, influenced the overall energy absorption capacity during lateral compression tests. The results showed that nested structures are effective in absorbing energy. Nested-tube energy absorbers tested under quasi-static loads were found to exhibit successful energy absorption performance during plastic deformation stages. In addition, numerical analyses indicated that these energy absorbers reduced blast loads by 50.1% to 74.3%. Complementing this study, Yang et al. [28] explored the integration of nested structures by inserting elliptical



tubes inside circular tubes, specifically targeting applications in aviation components. Their analysis delved into the lateral crushing behavior of these composite structures, concluding that the force–response curves of the circular and elliptical nested configurations exhibited greater stability compared to those composed solely of circular or elliptical tubes. This body of work underscores the significance of geometric optimization in enhancing the energy absorption efficiency of tubular structures under extreme loading conditions. Additionally, the combination of circular and elliptical shapes provides a structural advantage by improving stability and resistance to local buckling. The elliptical tube, in particular, enhances resistance to bending, while the circular tube offers radial strength.

Tubular structures, when augmented with foam fillings, exhibit a significantly enhanced capacity for energy absorption. The integration of foams as hybrid components alongside thin-walled tubes capitalizes on their inherent low density, ease of production, and superior specific energy absorption characteristics, as indicated in the literature [29]. In these studies, the foam filling significantly improves the crashworthiness of these structures by distributing crushing forces more efficiently, stabilizing the column walls, and preventing local buckling. These characteristics result in higher energy absorption and better structural integrity during collisions. The foam's presence enhances both the load-carrying capacity and the overall stability of the columns, making them more effective in crash scenarios. Overall, the foam acts as a crucial component in improving crashworthiness by distributing forces more effectively and enabling the structure to handle high-energy impacts more efficiently. In hybrid structures combining both foam and tubular elements, there is a notable increase in load bearing and energy dissipation capacities. This enhancement can be attributed to the synergistic interaction between the foam material and the walls of the tubes [30,31]. Moreover, foam-filled hybrid structures have been the subject of investigations within the context of nested tubes. In this realm, Xu et al. [32] conducted a comprehensive study on the behaviors of energy dissipation and lateral crushing for aluminum foam filled within nested aluminum tubes, specifically focusing on configurations comprising three and four tubes under compression testing scenarios. Additionally, Wang et al. [33] explored the crushing behavior of aluminum foam-filled steel circular and triangular nested tubes when subjected to lateral impacts. Their findings suggest that the incorporation of aluminum foam significantly bolsters the energy absorption capacity, mean crushing force, and collision force efficiency of the tubes, a phenomenon largely due to the interactive dynamics between the tube structure and the foam.

In contemporary vehicular engineering, growing emphasis is placed on the augmentation of component efficiency to mitigate fuel consumption and emission ratios [34]. Concurrently, the objective remains to preserve, if not enhance, the mechanical performance expected of these components. Given these ambitions, the prioritization of materials that exhibit both low density and high strength is paramount. In this context, composite materials have emerged as formidable contenders versus traditional metals such as steel and aluminum. This is attributed to their superior specific strength, reduced density, enhanced corrosion resistance, and the simplicity of their manufacturing processes [35,36]. However, the inherently brittle nature of composite materials introduces certain drawbacks. Specifically, their mode of energy absorption during collisions—through matrix cracking, fiber breakage, and delamination—precipitates abrupt reductions in their load-bearing capacity [36,37]. To counteract these vulnerabilities, strategies such as the development of hybrid composites incorporating metal structures and the reinforcement of composite tubes with cellular formations, including honeycomb and foams, are being explored. These innovations aim to imbue composite structures with a more resilient response to mechanical stresses [38].

As delineated in scholarly discourse, extensive research efforts have been dedicated to the development of metallic energy absorbers. Yet, the exploration of composite nested tubes as energy absorbers under lateral loading remains conspicuously absent in the existing literature. It has been observed that tubes with circular cross-sections deform into elliptical shapes upon lateral compression [39,40]. While metallic tubes dissipate energy at

the hinge points during lateral deformation, composite tubes exhibit fiber breakage and ruptures at their quarter points when subjected to lateral stress, thereby compromising their load-bearing capacity and diminishing their efficacy in energy absorption [41,42]. This phenomenon is similarly observed in foam-filled composite tubes, where the reduction in foam height—attributable to its transformation into an elliptical shape due to lateral compression—impedes the tube's contribution to load-bearing capacity [43]. To mitigate these adverse effects, a strategy has been proposed to delay the onset of fiber breakage and ruptures by encasing the composite tubes within expanded Polypropylene (EPP) blocks to restrict lateral deformation.

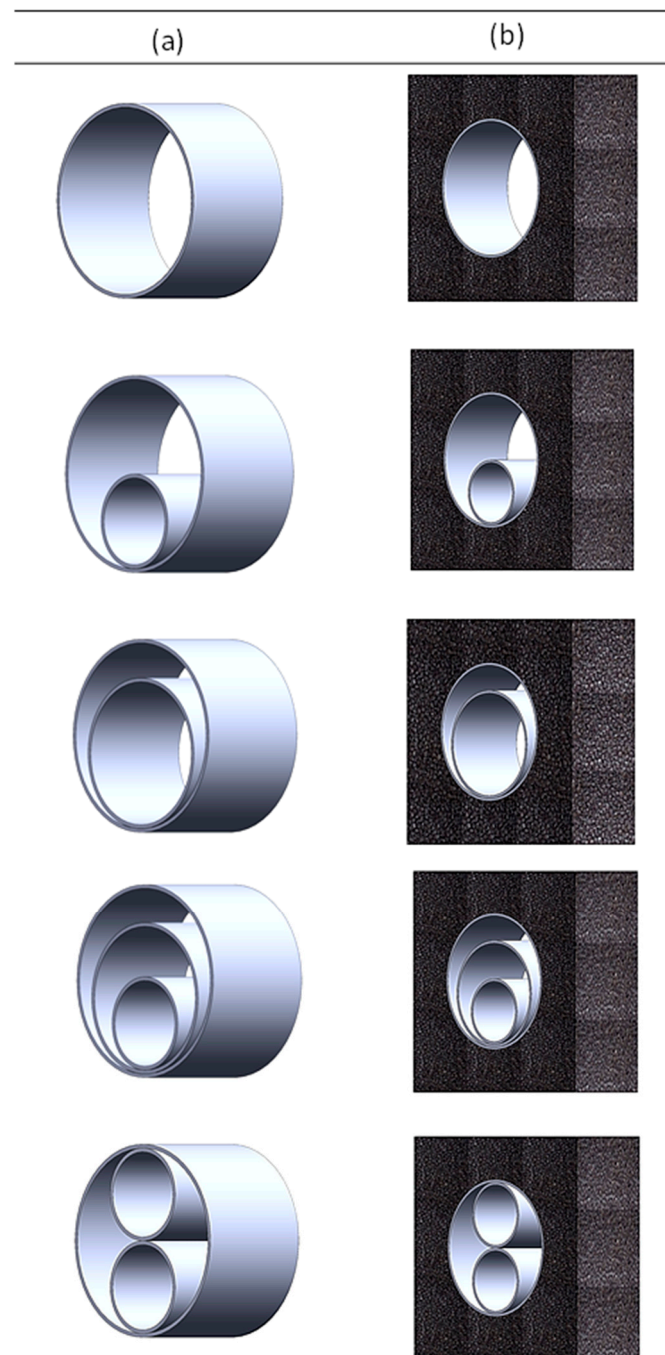
This study examines the energy efficiency and deformation behavior of EPP foam blocks reinforced with nested-tube reinforcements under quasi-static lateral loads. Previous discussions emphasize that foam is not a suitable filler material because of its poor energy efficiency, which is a result of the tubes' lateral expansion under these loading scenarios. In order to address this constraint, the current work creatively integrates CFRP and aluminum nested tubes into the EPP blocks. By severely limiting the tubes' lateral expansion under lateral pressure, this deliberate positioning is intended to improve the specimens' ability to absorb energy. It is evident from empirical findings that EPP foam specimens supplemented with nested-tube configurations perform significantly better in terms of crash efficiency than configurations in which nested tubes are used but EPP foam is not integrated. In particular, very good outcomes were obtained by combining lightweight nested CFRP tubes with EPP foam blocks. This study highlights the potential of lightweight composite materials in applications requiring high energy absorption and efficiency, while also adding to the body of knowledge by demonstrating the efficacy of nested-tube reinforcements in enhancing the energy absorption characteristics of EPP foam blocks.

## 2. Materials and Experimental Studies

In the fabrication of composite tubes, an epoxy resin known as “Sika CR 80” alongside a hardening agent, Sika CH 80-2, was employed, both of which were supplied by Dost Kimya Company, Istanbul, Turkey. This was complemented by the use of carbon fiber woven fabrics possessing an area density of  $200 \text{ g/m}^2$ . For the creation of metal tubes within the study, Al 6063-T4 alloys were selected due to their specific material properties. Additionally, EPP foam, characterized by a density of  $30 \text{ kg/m}^3$  and provided by Atermit Company, Sakarya, Turkey, was utilized in the construction process. The experimental setup involved the use of three distinct tube diameters to facilitate nested-tube combinations. These diameters were categorized as large (77 mm), medium (60 mm), and small (37 mm), respectively. The composite tubes themselves were meticulously crafted utilizing the hand lay-up technique. This method was performed on mandrels, employing brushes and rollers to ensure the uniform application and distribution of the resin and hardener components across the carbon fiber fabrics.

The fabrication of large-diameter tubes involved a process wherein the tubes were constructed by winding them around a two-piece polymer mold featuring a bolt–nut connection mechanism. Conversely, the production of medium- and small-diameter tubes was achieved by winding fibers around cylindrical cardboard tubes. To ensure that no adhesion occurred between the resin and the cardboard tubes, the latter were meticulously covered with tape. Following the initial construction phase, the composites were kept at room temperature for a duration of 24 h, subsequent to which a post-curing process was conducted in an oven maintained at a temperature of  $60^\circ\text{C}$  for 4 h. For the purpose of performing lateral crushing tests, the tubes were uniformly trimmed to a height 50 mm. A wetting process was employed to facilitate the separation of the cardboard from the composites, thus allowing for the isolation of medium- and small-diameter composites from their cardboard encasements. The adhesion of the tubes to one another was achieved through the application of an epoxy-based two-component adhesive, specifically Araldite 2011. In order to construct the nested-tube structures, these were installed within foam blocks measuring 130 mm by 115 mm. The configurations of these nested structures were

varied, encompassing both double- and triple-tube combinations along with their foamed variants, as illustrated in Figure 1. To elucidate the crushing behavior of these nested structures, compression tests were conducted utilizing an MTS 809 (Istanbul, Turkey) brand universal testing device, with the tests being performed at a velocity of 6 mm/min.



**Figure 1.** Arrangement of (a) nested tube-only and (b) nested-tube-reinforced EPP foam block specimens.

### 3. Crashworthiness Parameters

Energy absorbing structures are assessed based on their performance efficiency, employing multiple criteria including specific energy absorption capability, crush force efficiency, and overall energy efficiency [44,45]. Among these criteria, specific energy absorption (SEA) capability emerges as the paramount evaluation metric for energy absorbing

structures. SEA, which is defined as the amount of energy absorbed per unit weight, is articulated as illustrated in Equation (1).

$$SEA = \frac{EA}{m} \quad (1)$$

where  $m$  denotes the aggregate mass of the energy absorbing structure. Furthermore,  $EA$  represents the cumulative energy absorbed, which can be determined by calculating the area under the force–displacement curve of the structure. This calculation is facilitated through the utilization of the formula presented in Equation (2).

$$EA = \int_0^{\delta} F(\delta) \cdot d\delta \quad (2)$$

The parameters  $\delta$  and  $F$  represent displacement and force, respectively. The concept of the crushability ratio is elucidated as the quotient obtained by dividing the displacement value, recorded at the conclusion of the experimental procedure, by the initial diameter of the structure under investigation. This is formally expressed in Equation (3).

$$e_g = \frac{l}{d} \quad (3)$$

The parameters of  $l$  and  $d$ , denoting the crushed and original length of the absorber, are critical in this evaluation. The concept of work effectiveness ( $W_{eff}$ ) encompasses both the specific energy absorption capacity and the crush efficiency indicator. This parameter is essential in evaluating the performance of energy absorbers, offering a comprehensive measure that combines both energy absorption efficiency and structural integrity post deformation.

$$W_{eff} = SEA \times e_g \quad (4)$$

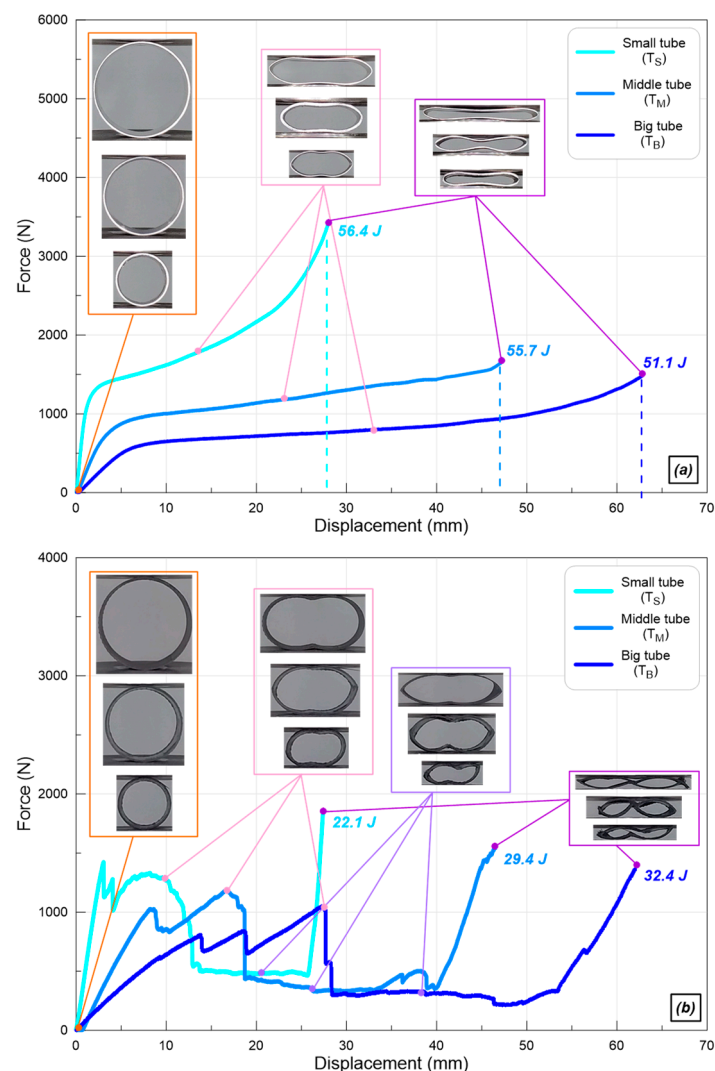
#### 4. Results and Discussion

The study conducted experiments on both single tubes and nested specimens to test their lateral crushing capabilities. Each sample group underwent three separate tests to ensure accurate and reliable results. To minimize visual confusion, the average degree curve was used as the final result for each sample group. Additionally, experiments for each specimen group were stopped at a displacement value equal to 85% of the maximum crushing capacity, preventing any damage to the equipment or specimens.

##### 4.1. Single Tubes

The force–displacement profiles and the progressive deformation stages derived from lateral crush testing of aluminum and carbon fiber-reinforced polymer (CFRP) single tubes are illustrated in Figure 2. It is imperative to underscore that the force profiles for both aluminum and CFRP tubes exhibit congruence with prior studies documented in the literature, notwithstanding the observation that each material's force profile presents distinct characteristics, albeit homogeneity within their respective groups is observed. A notable aspect is the rapid increase in force profiles at the onset of the experiments, characterized by a steep slope. This rate of force escalation at the experiment's commencement inversely correlates with the diameter of the tubes, irrespective of the material composition. Consequently, the initiation of deformation in the specimens was observed at the lowest force value in the tube possessing the largest diameter, similar to results in the literature [46]. This phenomenon, where a higher moment—and therefore force—is necessitated to initiate deformation in tubes of diminishing diameters, accounts for the aforementioned force variation. In contrast to CFRP tubes, aluminum tubes maintained their load-bearing capacity post the initial deformation. The diminished load-bearing capability observed in CFRP tubes can be ascribed to the inherent layered structure of composite materials and their comparative brittleness

compared to metal counterparts. Indeed, while brittle composite tubes exhibiting lower deformability commenced deformation at elevated force values relative to their metallic counterparts, they subsequently underwent a near-complete loss of load-carrying capacity within a brief duration. This phenomenon markedly influenced the energy absorption metrics of the tubes, with absorbed energy values in aluminum tubes delineating a decrease from 56.4 J, 55.7 J, and 51.1 J across specimens of increasing diameters ( $T_S$ - $T_M$ - $T_B$ ), to 22.1 J, 29.4 J, and 32.4 J in CFRP tubes. This attenuation in load-carrying capacity engendered a reversal in the trend in energy absorption behavior, which in aluminum tubes escalated with decreasing diameter, a trend that was inverted in CFRP tubes. If the characteristics of metal and composite curves are examined, aluminum tube structures absorb energy due to the high ductility behaviors and superior plastic deformation capabilities of metals, while the curves are formed in a smooth form. However, composite materials absorb crushing energy with damage mechanisms such as matrix cracking, local buckling of fibers, fiber breakage, and delamination. Due to these fiber breaks, oscillations occur in the curves of composite structures [47,48].



**Figure 2.** The force–displacement curves of single (a) aluminum and (b) CFRP tubes under a lateral crushing load.

#### 4.2. Nested Tubes

The findings from the lateral compression examinations of composite samples, consisting of dual and triple aluminum tubing configurations, are delineated in Figure 3. The

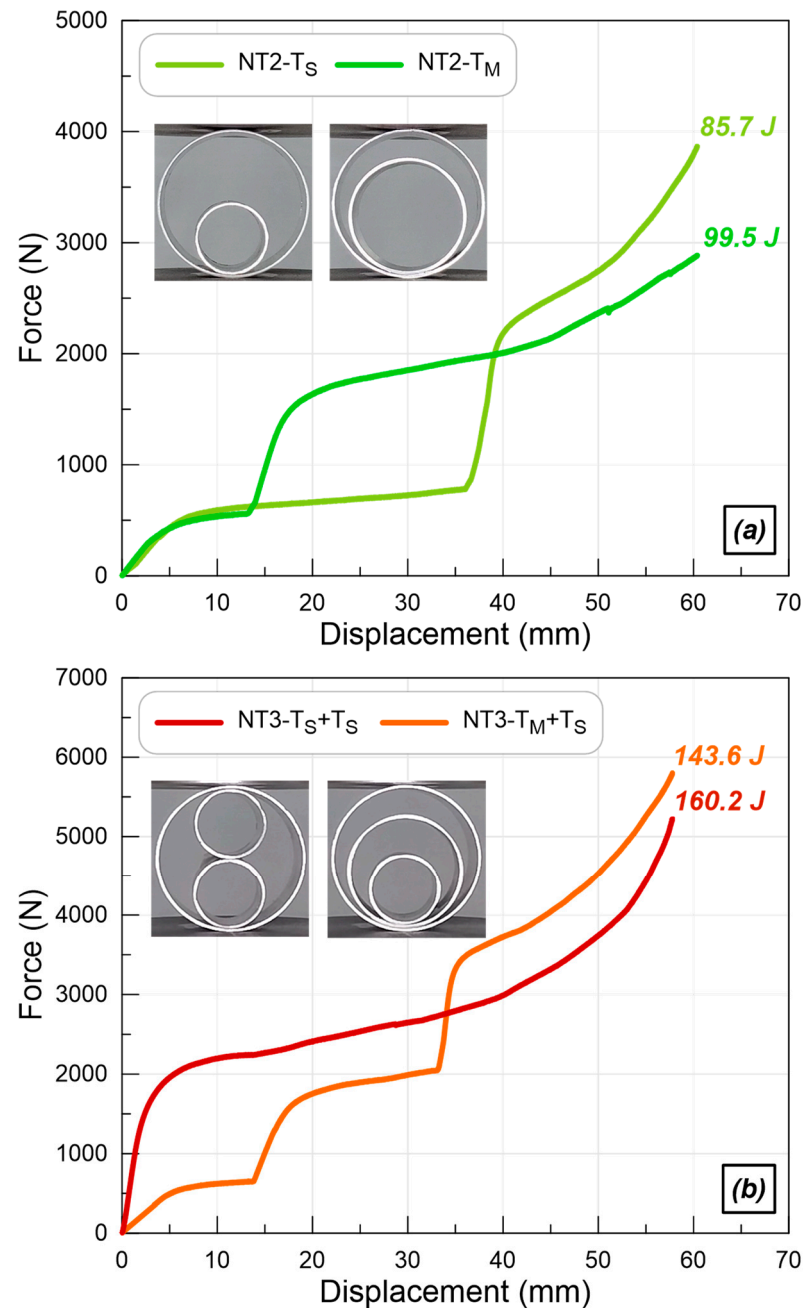


bi-tubular samples were fabricated by inserting tubes of small ( $T_S$ ) and medium ( $T_M$ ) dimensions into a larger tube, whereas the tri-tubular specimens were constructed by incorporating either two small tubes or one small and one medium tube within a large tube. An epoxy-based adhesive was employed to preserve the original positioning of the tubes during the lateral compression test. In the case of the bi-tubular specimens, the spatial separation between the outer surface of the  $T_S$  and  $T_M$  tubes and the inner surface of the large tube measured at 37 mm and 14 mm, respectively. Additionally, a 20 mm gap was observed between the  $T_S$  and  $T_M$  tubes. The dimensional selection of the tubes, allowing for the accommodation of two smaller tubes within the larger tube, was a critical consideration. Upon analysis of the force–displacement graphs presented in Figure 3a, it is observed that the force profiles initially align with those of the  $T_B$  tube. However, post a specific displacement threshold, the nature of the force curve alters. This suggests that deformation initially occurs solely within the  $T_B$  tube, and subsequently, as the  $T_B$  tube comes into contact with the inner tube(s), the combined deformation of these tubes results in the modification of the force curve. Utilizing the  $T_M$  tube internally results in a rapid escalation in the force curve at approximately 14 mm of displacement, akin to the initial response observed in the  $T_M$  single-tube experiment. Conversely, when a  $T_S$  tube is incorporated (in the NT2- $T_S$  sample), this escalation is noted at a displacement of roughly 37 mm. The emergence of a stepped force curve through the integration of tubes of varying diameters is significantly noteworthy as it demonstrates the potential for deliberate manipulation of the force curve. Given that the NT2- $T_M$  specimen exhibits an energy absorption capacity approximately 16% higher than that of the NT2- $T_S$  specimen, it is inferred that an earlier onset of the stepped force curve phenomenon is preferable.

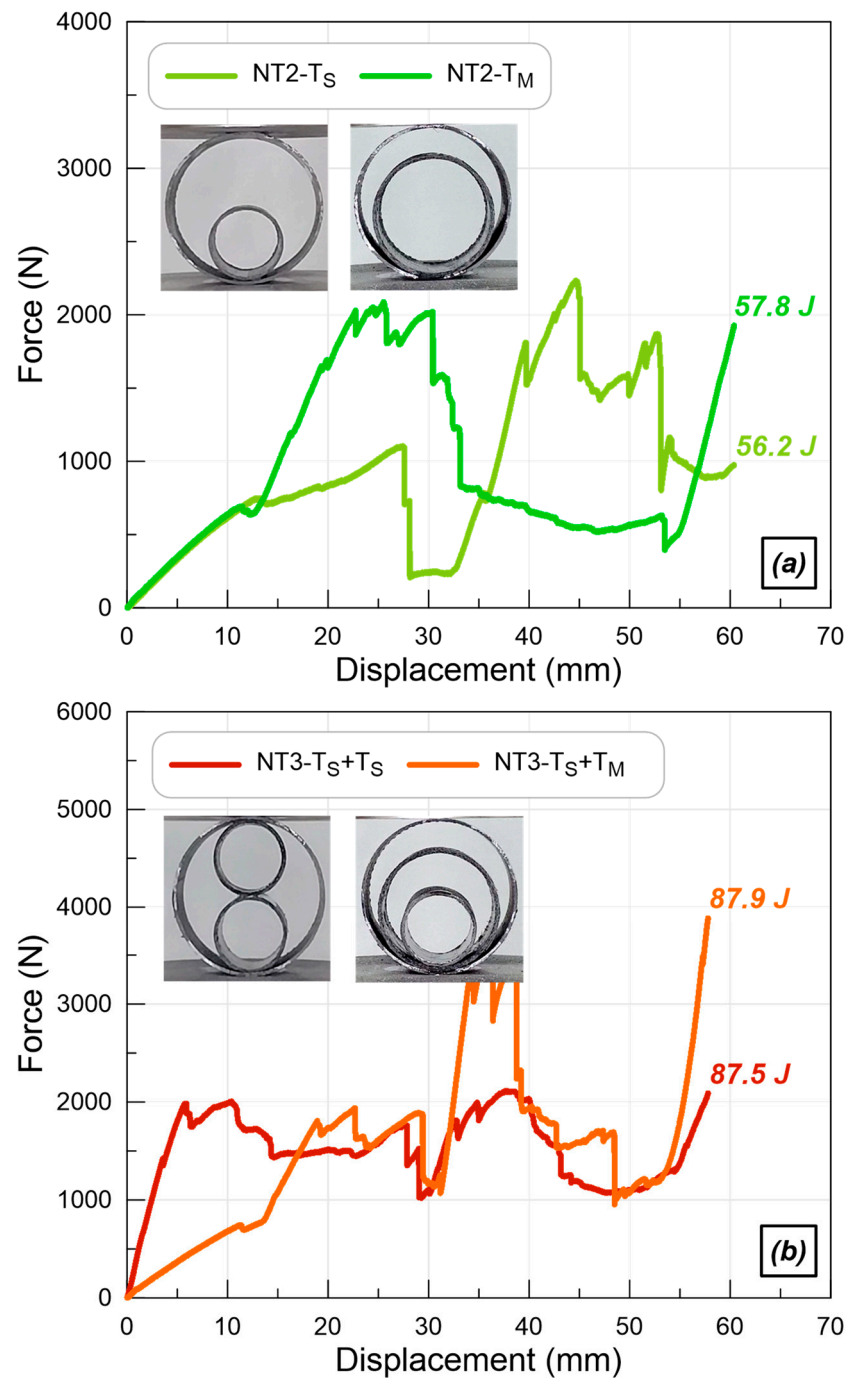
The stepped structure of the force curve, previously mentioned, exhibits a more pronounced character in the NT3- $T_S$ + $T_M$  specimen, as delineated in Figure 3b. Initially, deformation occurs in the larger tube, succeeded by the  $T_M$  tube's deformation at approximately 14 mm, culminating in the emergence of the initial step; the subsequent step materializes with the  $T_S$  tube's deformation at around 34 mm. In juxtaposition, the NT2- $T_S$  specimen evidences an escalation in the force curve at a displacement value of 37 mm. However, this value markedly diminishes to 14 mm in the NT3- $T_S$ + $T_M$  specimen, a phenomenon likely attributable to the concurrent deployment of the  $T_S$  and  $T_M$  tubes within the triply nested specimen. Conversely, the NT3- $T_S$ + $T_S$  specimen, employing two  $T_S$  tubes, does not exhibit a stepped force curve, maintaining uniformity akin to the force curves observed in single-tube specimens, as illustrated in Figure 3b. This uniformity arises from the inner tubes' interaction with the  $T_B$  tube, facilitating a more consistent force curve and enabling a 12% enhancement in energy absorption at the experiment's inception. Given the dual incorporation of smaller tubes in the NT3- $T_S$ + $T_S$  specimen, it is anticipated that a higher specific energy value will be achieved, correlating with a reduced sample weight compared to the NT3- $T_S$ + $T_M$  specimen.

The preceding text outlines the results from lateral crushing tests performed on nested CFRP composite specimens, as seen in the cited pictures (Figure 4). The experimental data primarily examine the force–displacement characteristics of both two-tube and three-tube CFRP composite specimens, with a comparison versus their aluminum counterparts. The early deformation phase is notably comparable across different specimens, due to the primary deformation of the  $T_B$  specimen, which reflects the behavior seen in aluminum tubes. The differences in the force curves resulting from initial contact versus non-contact with the main tube are distinctly seen in the graphs. This phenomenon is particularly pronounced in specimens featuring three tubes; nonetheless, the initial congruence of the force curves in the absence of contact (Figure 4a) is also significant as it demonstrates the efficient manufacturing of the CFRP tubes. The story clarifies the specimens' dynamic response to a load, emphasizing the cyclical adaptation of force due to gradual structural compromise and the consequent involvement of the smaller tube in the deformation process. The discussion highlights a unique energy absorption pattern between the two-tube and three-tube specimens, with the latter exhibiting a more stable force curve, despite

closely comparable energy absorption levels, differing from the behavior seen in the aluminum tubes. This exposition emphasizes the intricate behavioral characteristics of CFRP composite tubes during lateral crushing and contributes to the wider discussion on the structural integrity and durability of composite materials in load-bearing applications.



**Figure 3.** The force–displacement curves of nested aluminum (a) two-tube and (b) three-tube samples under a lateral crushing load.



**Figure 4.** The force–displacement curves of nested CFRP (a) two-tube and (b) three-tube samples under a lateral crushing load.

The progressive deformation stages of the nested aluminum samples, comprising configurations with two and three tubes, are detailed in Table 1. Initially, deformation begins in the largest aluminum tube for all samples, except for the nested sample containing two smaller tubes. The outermost tube starts to deform under the applied load until it contacts the inner tube. Once contact is made, the deformation propagates to the inner tube, causing it to deform as well. This sequential deformation pattern creates force curves characterized by distinct steps, each corresponding to the different stages of deformation in the nested structure. Similarly, the nested samples made from carbon fiber-reinforced polymer (CFRP) exhibit a progressive deformation pattern. However, due to the brittle nature of CFRP, these tubes experience cracking as deformation progresses. The cracks

appear on the tube walls once the deformation reaches a certain threshold. Notably, the sequence of cracking is consistent across all CFRP tubes, irrespective of their diameter. Cracks first develop at the upper and lower sections of the tube and subsequently at the right and left sides. This cracking sequence significantly impacts the load-bearing capacity of the nested CFRP samples, leading to abrupt reductions in force. These sudden drops are evident in the force–displacement curves of the CFRP samples, as illustrated in Figure 4. The contrasting behavior between aluminum and CFRP tubes is further highlighted in the smooth force curves observed for the aluminum samples (Figure 3). The absence of cracking in the aluminum tubes is attributed to their ductile behavior, which allows them to undergo significant deformation without sudden failure. This ductility ensures a more gradual and continuous absorption of energy, resulting in smoother force–displacement curves compared to the CFRP samples. In conclusion, the progressive deformation behavior of nested aluminum and CFRP tubes demonstrates distinct characteristics influenced by the material properties. The stepped force curves of the aluminum samples are indicative of a sequential deformation process without sudden failure, while the force–displacement curves of the CFRP samples reflect the brittle nature of the material, marked by sudden drops due to cracking. Understanding these deformation mechanisms is crucial for optimizing the design and performance of nested tubular structures in various engineering applications.

Table 1. Deformation stages of nested aluminum and CFRP samples.

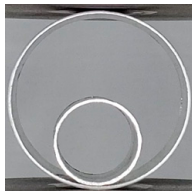



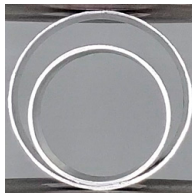







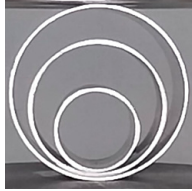



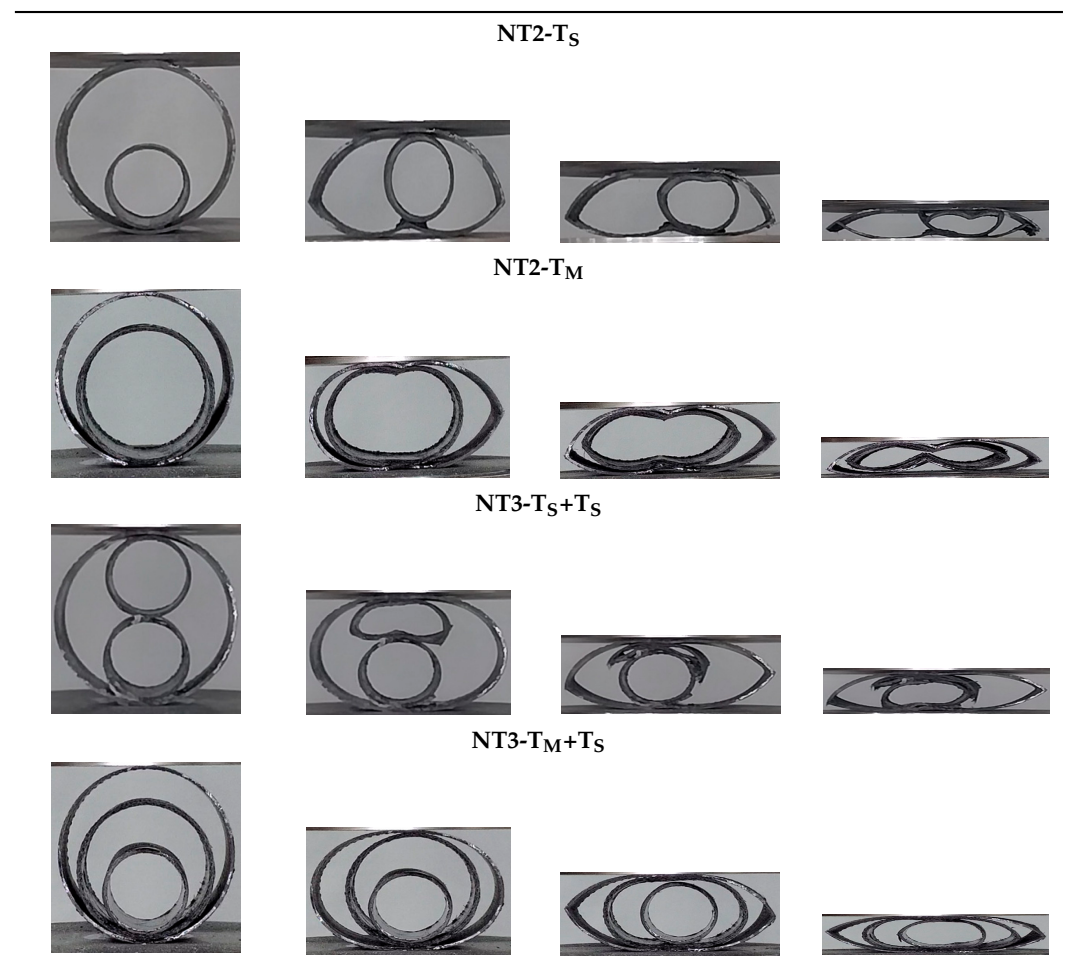
NT2-T <sub>S</sub>				
				
NT2-T <sub>M</sub>				
				
NT3-T <sub>S</sub> +T <sub>S</sub>				
				
NT3-T <sub>M</sub> +T <sub>S</sub>				
				

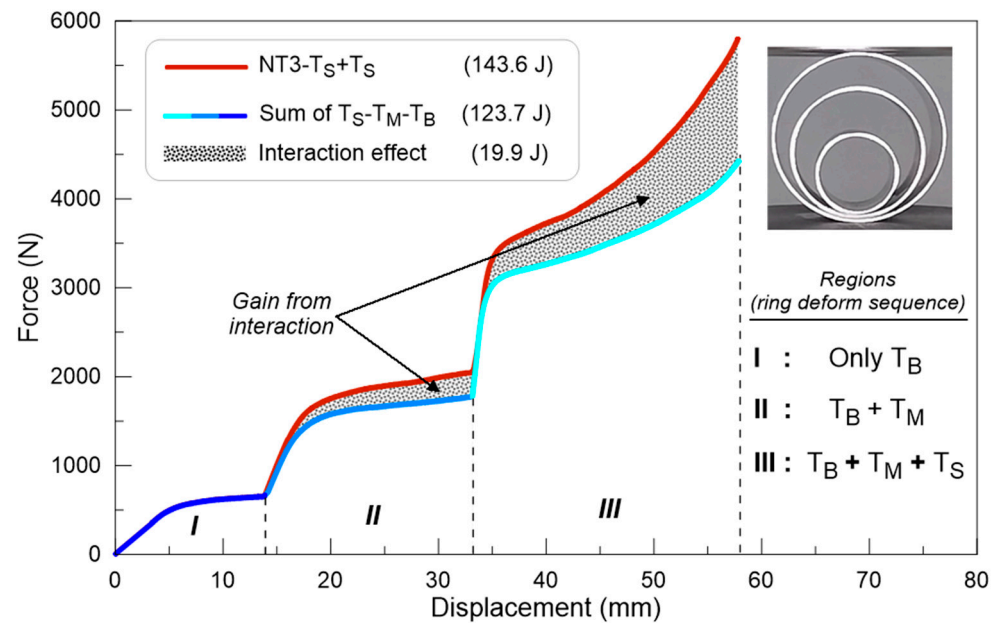
Table 1. Cont.



#### 4.3. The Interaction Occurred in the Nested Sample

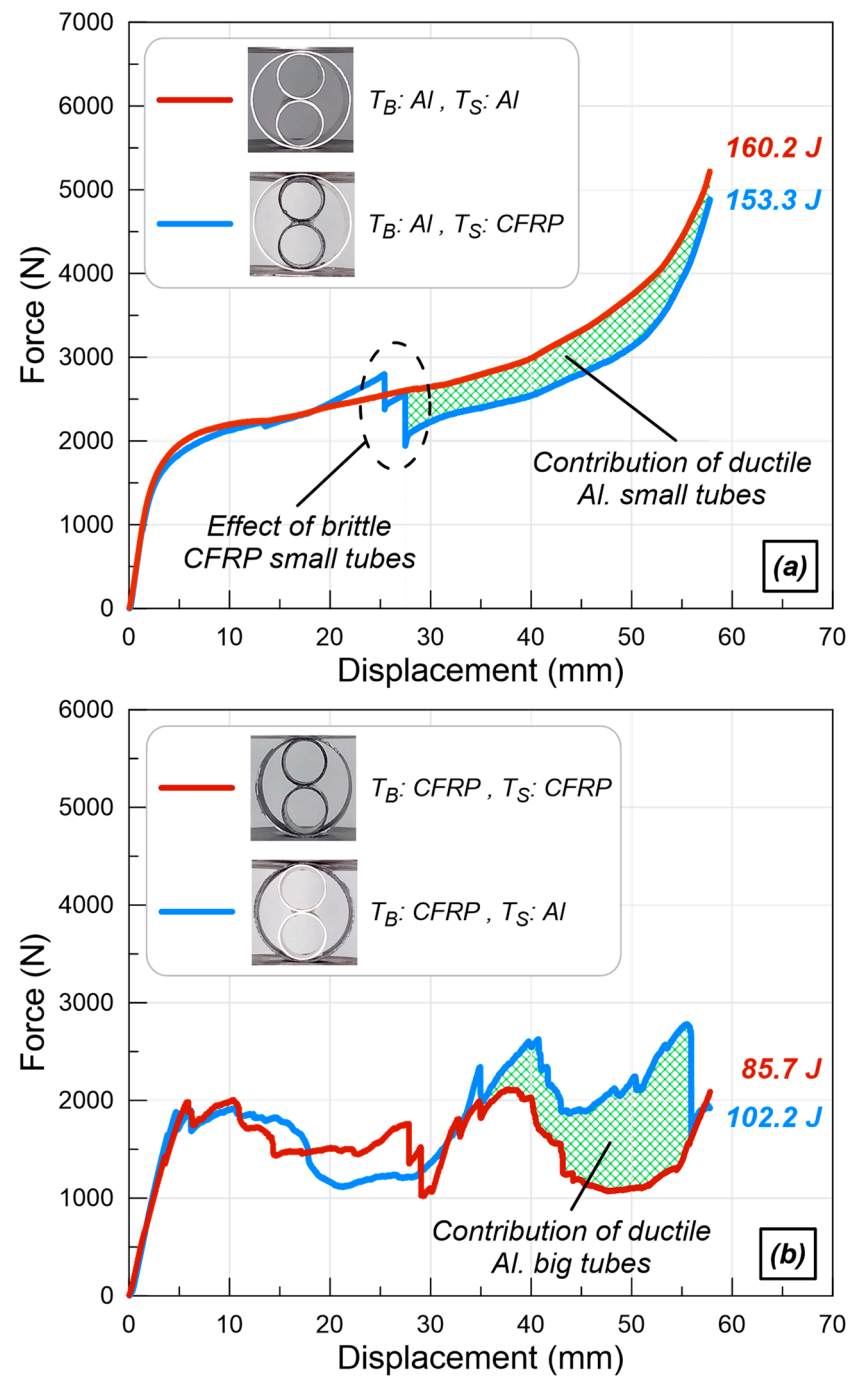
The deformation of tubes arranged in nested configurations leads to interactive phenomena that substantially affect the energy absorption properties of these structures. In this context, the force–displacement characteristics of the NT3- $T_S+T_M$  specimen, along with the force curves corresponding to the individual tubes that constitute this specimen, are collectively illustrated in Figure 5. The force curve associated with the NT3- $T_S+T_M$  sample is clearly represented in a maroon color within the figure, contrasting with the force curves of the individual tubes, which are depicted in different shades of blue (specifically blue, dodger blue, and cyan) to enhance differentiation. The segmentation of the force curve into three distinct parts clarifies the sequential deformation processes encountered by tubes of different dimensions. The initial segment specifically illustrates the deformation occurring in the largest tube alone, while the following segments indicate the gradual involvement of the medium and smallest tubes in the deformation process, respectively. The force curve for each individual tube was derived by algebraically summing the initial force values associated with each tube, starting from the force value recorded in the previous section. The NT3- $T_S+T_M$  specimen demonstrated a significant increase in energy absorption, amounting to 19.9 J, when compared to the total energy absorbed by the individual tubes at the same displacement threshold. Additionally, the assessment of the maximum crush displacement metric was based on the highest crush displacement recorded in the tri-tubular specimen configuration.





**Figure 5.** The interaction between the single tubes when deforming together in the nested sample NT3-TS+TS.

In the context of three-tube nested specimens, the investigation extends to configurations wherein tubes are fabricated from dissimilar materials, scrutinizing the resultant interactions as previously delineated. The subsequent figures (referenced as Figure 6) delineate the force–displacement trajectories for specimens characterized by the employment of  $T_B$  and  $T_S$  tubes composed of heterogeneous materials. Specifically, Figure 6a illustrates a composite of aluminum  $T_B$  and CFRP  $T_S$  tubes, whereas Figure 6b depicts the inverse material configuration. Notably, Figure 6a reveals a precipitous decline in the force curve at approximately 25 mm of displacement when CFRP tubes are utilized internally—a phenomenon absent in specimens comprising aluminum analogs. This decline is attributable to fractures manifesting on the lateral aspects of the CFRP  $T_S$  tubes, engendering a 4% reduction in energy absorption capacity of the specimen. Furthermore, the incorporation of CFRP  $T_S$  tubes results in a substantial mass reduction exceeding 27%, enhancing the specimen's overall efficiency. Conversely, the specimen illustrated in Figure 6b, despite the decrement in absorbed energy due to the substitution of aluminum  $T_S$  tubes with CFRP, experiences a compensatory reduction in mass that ostensibly mitigates the impact of reduced energy absorption. The juxtaposition of different material tubes not only influences the absolute energy absorption but also significantly affects the energy absorption efficiency. Intriguingly, specimens evidencing a decline in absorbed energy exhibit enhanced specific energy absorption capabilities relative to their original configuration. Conversely, an augmentation in absorbed energy correlates with a diminution in specific energy values. Consequently, this suggests that the pivotal metric in evaluating energy absorbing structures is not merely the quantum of energy absorbed but rather the efficiency with which this energy is assimilated.



**Figure 6.** The force-displacement curves of three tube nested samples (a) small tubes of CFRP and Al placed in Al outer tube, (b) small CFRP and Al tubes placed in CFRP outer tube.

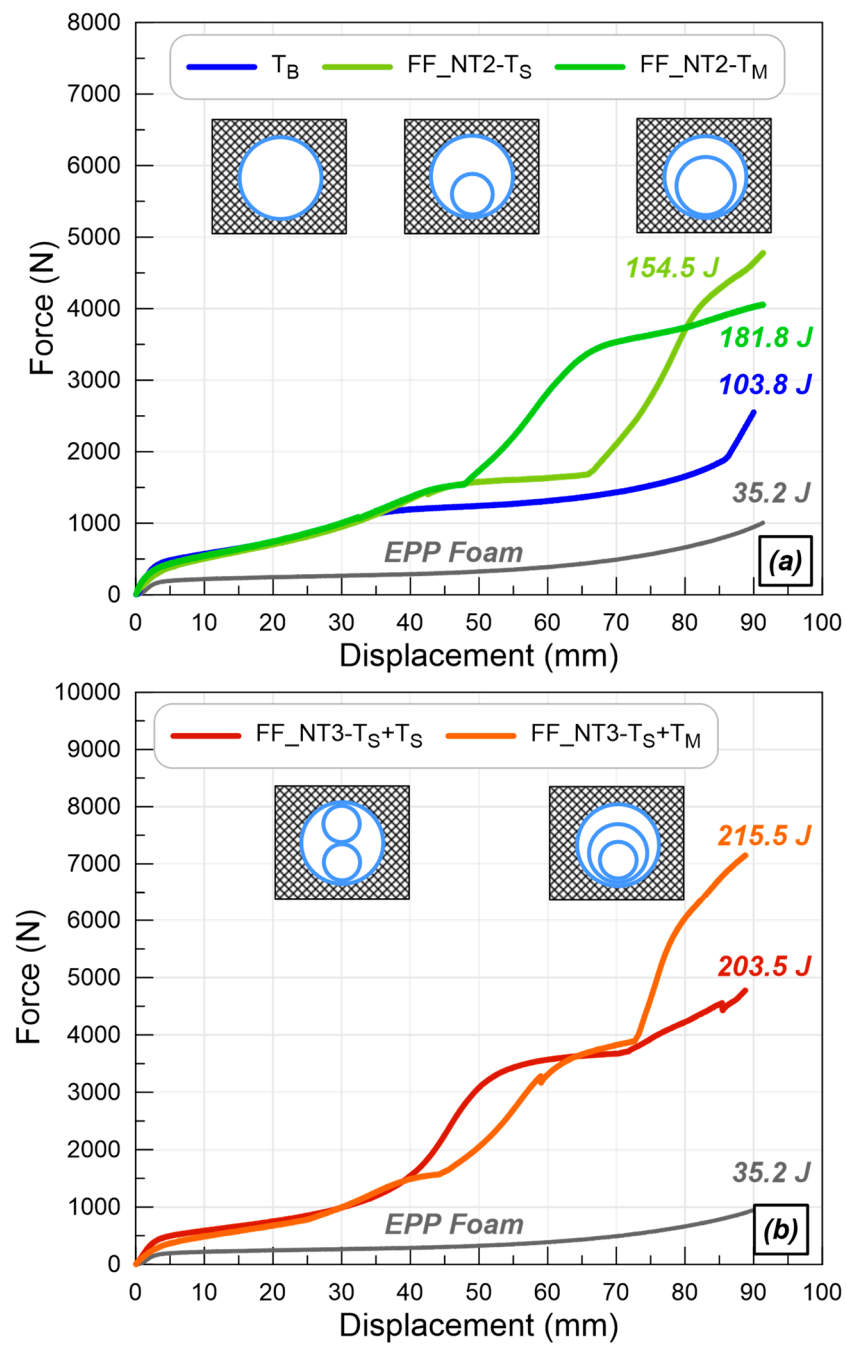
#### 4.4. Nested Tube-Reinforced EPP Foams

This section presents the findings of testing EPP foam blocks reinforced with aluminum and CFRP composite nested tubes under in-plane crushing stresses. The EPP foam blocks employed in this investigation are consistent in terms of dimensions, each measuring 130 mm by 115 mm, with a density of 30 kg/m<sup>3</sup>. Only the tubes with a larger diameter were chosen to reinforce the EPP foam. Due to the considerably greater strength of both aluminum and CFRP composite tubes relative to EPP foam, no appreciable deformation of the tubes was detected until a displacement of about 35 mm was attained from the commencement of the testing procedure. Following this displacement threshold, a progressive increase in the force curve was recorded, as illustrated in Figures 7 and 8.

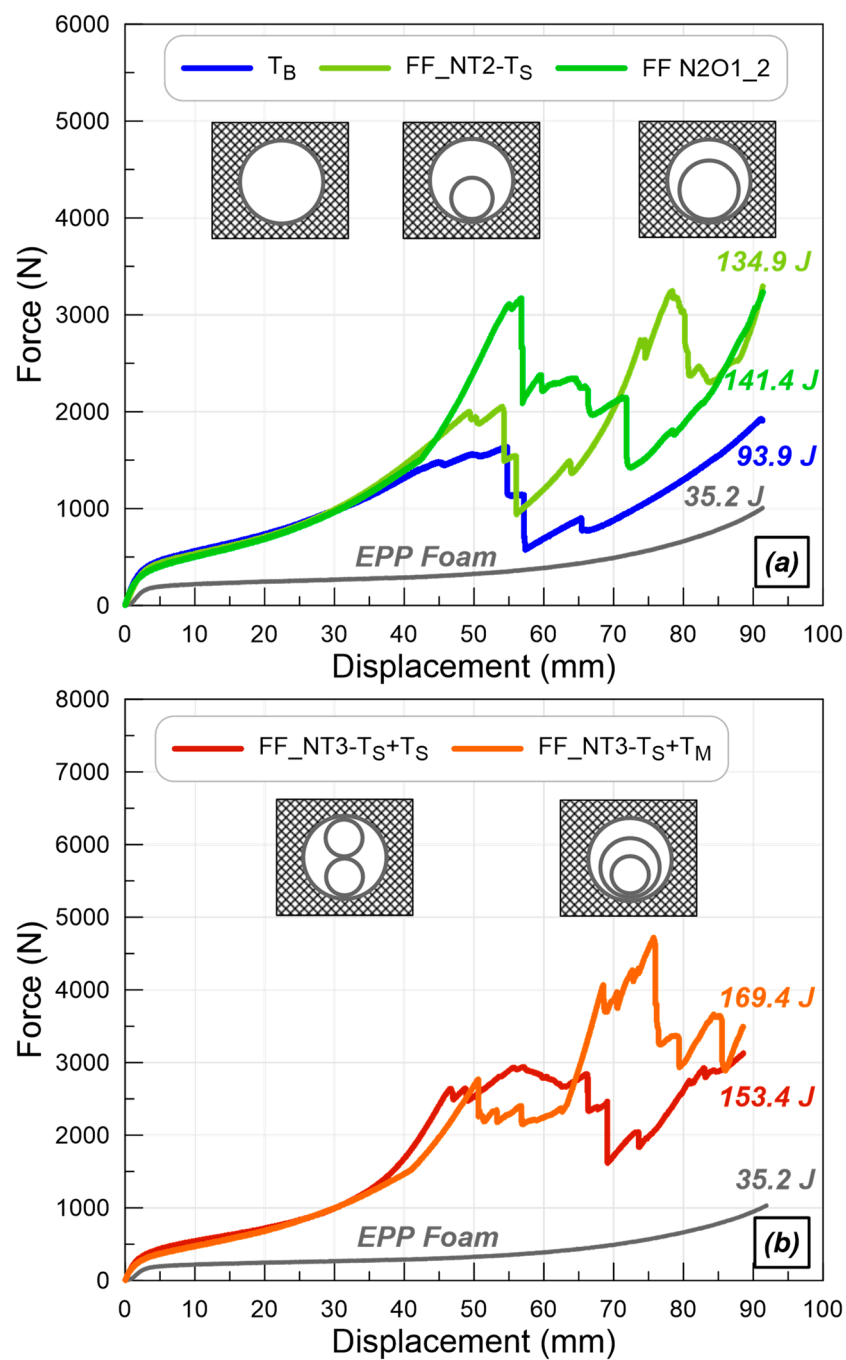
Furthermore, it is noteworthy that above this displacement threshold, the force curves increase at a reduced gradient compared to those observed for both aluminum and CFRP composite tubes without EPP foam reinforcement. The deformation curves for the double and triple nested tubes, depicted in Figure 7, demonstrate the emergence of distinctive force curves for the nested specimens, similar to those shown in Figures 3 and 4, after an average displacement of 40 mm. A consistent trend is evident in the force curves of the CFRP tubes, as illustrated in Figure 8. The force values for both aluminum and CFRP composite tubes increase by an average of 1000 N with the addition of EPP foam. Analysis of the energy absorption values of the specimens revealed a significant increase in EPP foam, exceeding the total energy values of both the specimen and the foam. This result is notably significant, reflecting the interaction effect seen when individual tubes are employed together. The single  $T_B$  tube and EPP foam exhibited energy absorption values of 51.1 J and 35.2 J, respectively, totaling 86.3 J, whereas the  $FF\_T_B$  sample showed a 20% enhancement in energy absorption, as illustrated in Figures 2a and 7a. The increase was particularly significant in the CFRP composite  $T_B$  tube, reaching approximately 39%, as illustrated in Figures 2b and 8a. The maximum and minimum improvements in energy absorption from interactions in the nested-tube-reinforced EPP foam specimens were observed in the  $FF\_NT2-T_M$  and  $FF\_NT3-T_S+T_S$  samples, with enhancements of 35% and 5% for aluminum and 25% and 52% for CFRP composite, respectively. Furthermore, the increase in energy absorption for all nested CFRP composite tube-reinforced specimens surpassed that recorded in specimens reinforced with nested aluminum tubes.

Following the completion of experiments on the nested samples, the EPP foam blocks were reinforced with nested aluminum and CFRP tubes and underwent compression testing. The main aim of this reinforcing method was to restrict the lateral expansion of the aluminum and CFRP tubes, thus improving the energy absorption capacity of the samples. The compressive deformation behavior of the EPP foam blocks was meticulously examined. The findings in Table 2 demonstrate that the EPP foam blocks underwent considerable expansion when exposed to compressive stresses. This deformation was directly linked to the lateral expansion of the outer tube. The strengthening of EPP foam sought to limit lateral expansion, thus enhancing the structural integrity and energy absorption capabilities of the nested tubes. A comprehensive comparison of the force–displacement curves between the nested samples and the nested-tube-reinforced EPP foam samples demonstrated significant differences. The use of EPP foam led to an increase in the crushing displacement of the samples by roughly 30 mm. This research demonstrates that the EPP foam permitted more deformation prior to failure, which is essential for applications necessitating high energy absorption. Moreover, the examination of the force–displacement curves indicated that the plateau and maximum force values of the nested samples were markedly increased with the inclusion of EPP foam. The plateau force, indicative of the sustained force level during deformation, was elevated, signifying an improved capacity to absorb energy over an extended displacement. Correspondingly, the maximum force value, indicative of the peak load the sample can endure prior to failure, was elevated, illustrating the enhanced strength of the reinforced samples. The results highlight the substantial role of EPP foam in enhancing the energy absorption capacity of the nested samples. The augmented crushing displacement and heightened force values indicate that EPP foam significantly improves the mechanical properties of the nested-tube constructions. The enhancement in energy absorption capability has significant implications for the design and development of sophisticated materials and structures across numerous engineering applications, especially in domains where impact resistance and energy dissipation are crucial. The reinforcement of nested aluminum and CFRP tubes with EPP foam blocks greatly improves the energy absorption capacity of the samples. The experimental findings indicate that EPP foam can enhance the mechanical performance of nested-tube constructions, positioning it as a promising material for applications necessitating high impact resistance and energy absorption. Future research should investigate the optimization of EPP foam characteristics

and reinforcement combinations to further improve the performance of these composite structures.



**Figure 7.** Force–displacement curves of nested aluminum (a) two-tube- and (b) three-tube-reinforced EPP foam blocks under in-plane loading.



**Figure 8.** Force–displacement curves of nested CFRP (a) two-tube- and (b) three-tube- reinforced EPP foam blocks under in-plane loading.

**Table 2.** Deformation stages of nested aluminum and CFRP tube-reinforced EPP foam blocks.





Table 2. Cont.

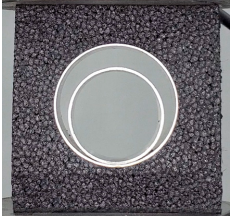




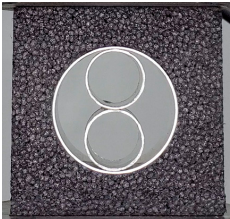


















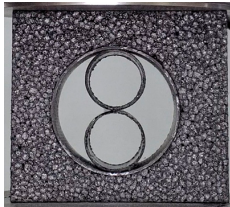








FF_NT2-TM				
				
FF_NT3-T <sub>S</sub> +T <sub>S</sub>				
				
FF_NT3-T <sub>S</sub> +T <sub>M</sub>				
				
FF_NT2-T <sub>S</sub>				
				
FF_NT2-T <sub>M</sub>				
				
FF_NT3-T <sub>S</sub> +T <sub>S</sub>				
				

Table 2. Cont.

FF_NT3-T <sub>S</sub> +T <sub>M</sub>				
				

#### 4.5. Crashworthiness

The findings of the experimental study, inclusive of all utilized specimens and specific crashworthiness parameters, are comprehensively delineated in Table 3. This table elucidates a discernible variance in the force exerted by specimens contingent upon the material composition. It is observed that both the mean and peak force metrics for the single and nested CFRP composite tubes are markedly inferior to those of their aluminum counterparts across all specimen configurations. This discrepancy is attributed to the brittle nature of carbon fiber composites, which detrimentally impacts the specimens' capacity to bear loads. Furthermore, the crushability indices of the samples exhibited variability correlating to the quantity of tubes employed. For singular tubes, the crushability index was ascertained through the calculation of the ratio of 85% of the tube's inner diameter to its outer diameter. The method for determining the crushability of nested samples adhered to a similar paradigm. Nonetheless, a distinct approach was employed for nested samples wherein 85% of the value derived from subtracting the cumulative wall thickness of the interior tubes from the inner diameter of the TB tube was established as the sample's crushability ratio. Consequently, an inverse relationship between the crushability ratio and the number of tubes in the nested samples is anticipated. Independent of material composition, it was noted that tubes of smaller diameter exhibited superior maximum force values relative to their larger counterparts. This phenomenon aligns with the premise that the force requisite to deform a specimen should escalate inversely with its diameter. Evidently, the maximum force values recorded for the nested specimens utilizing the T<sub>S</sub> tube significantly surpassed those of specimens employing the T<sub>M</sub> tube, a trend that was consistent among specimens integrated with EPP foam.

The outcomes derived from the utilization of various specimens within the experimental framework, alongside associated crashworthiness metrics, are systematically documented in Table 1. This tabulation elucidates a pronounced disparity in the force exerted by specimens based on their material composition. Specifically, both average and maximum force exertions by single and nested carbon fiber-reinforced polymer (CFRP) composite tubes were observed to be inferior to those of their aluminum analogs across all specimen configurations. This phenomenon can be attributed to the brittle character of the carbon fiber composite, which negatively impacts the load-bearing efficacy of the specimen. Additionally, the crushability indices of the samples manifested variations contingent upon the number of tubes employed. For individual tubes, the crushability index was derived by calculating the ratio of 85% of the inner diameter to the outer diameter of the tube. The computation of crushability for nested configurations adhered to a similar methodology. However, for nested samples, 85% of the resultant value obtained by subtracting the aggregate wall thickness of the internal tubes from the inner diameter of the T<sub>B</sub> tube was designated as the crushability ratio for the sample. Consequently, an augmentation in the number of tubes within nested configurations is anticipated to affect the crushability ratio inversely. Irrespective of the material composition, the maximum force value associated with tubes of smaller diameters surpassed those of larger diameters. This observation corroborates the hypothesis that a decrease in diameter necessitates an increase in the force required to deform the specimen. Indeed, the maximum force values for nested specimens

utilizing the  $T_S$  tube significantly exceeded those involving the  $T_M$  tube, a pattern that remained consistent for specimens incorporating EPP foam.

**Table 3.** The crashworthiness results of samples used in the experimental study.

Sample Combination			Crushability Ratio, e.g., (mm/mm)	Sample Weight (g)	Fmean (N)	Fmax (N)	Absorbed Energy, EA, (J)	Specific Energy Absorption, SEA, (J/g)	Crush Force Efficiency, CFE, (%)	Work Effectiveness, Weff, (J/g)
Aluminum based samples	Single rings	$T_B$	0.82	46.5	812	1491	51.1	1.10	54	0.90
		$T_M$	0.81	39.2	1150	1640	55.7	1.42	70	1.15
		$T_S$	0.78	23.3	1952	4141	56.4	2.42	47	1.89
	Nested tube samples	NT2- $T_S$	0.78	69.8	1420	3865	85.7	1.23	37	0.96
		NT2- $T_M$	0.78	85.7	1649	2884	99.5	1.16	57	0.91
		NT3- $T_S$ + $T_S$	0.75	93.1	2772	5219	160.2	1.72	53	1.29
		NT3- $T_S$ + $T_M$	0.75	109	2484	5799	143.6	1.32	43	0.99
	Nested tube reinforced EPP foam	FF- $T_B$	0.82	59.2	1105	2550	103.8	1.75	43	1.43
		FF-NT2- $T_S$	0.78	82.5	1692	4781	154.6	1.87	35	1.47
		FF-NT2- $T_M$	0.78	98.4	1990	4058	181.8	1.85	49	1.45
		FF-NT3- $T_S$ + $T_S$	0.75	105.8	2292	4774	203.5	1.92	48	1.44
		FF-NT3- $T_S$ + $T_M$	0.75	121.8	2427	7148	215.5	1.77	34	1.33
CFRP based samples	Single rings	$T_B$	0.82	25.3	515	1367	32.4	1.28	38	1.05
		$T_M$	0.81	20.5	607	1544	29.4	1.43	39	1.16
		$T_S$	0.78	10.6	765	1858	22.1	2.08	41	1.63
	Nested tube samples	NT2- $T_S$	0.78	35.9	931	2234	56.2	1.57	42	1.23
		NT2- $T_M$	0.78	45.8	958	2087	57.8	1.26	46	0.99
		NT3- $T_S$ + $T_S$	0.75	46.5	1514	2113	87.5	1.88	72	1.41
		NT3- $T_S$ + $T_M$	0.75	56.4	1521	3886	87.9	1.56	39	1.17
	Nested tube reinforced EPP foam	FF- $T_B$	0.82	38	1000	1925	93.9	2.47	52	2.02
		FF-NT2- $T_S$	0.78	48.6	1477	3295	134.9	2.78	45	2.18
		FF-NT2- $T_M$	0.78	58.5	1548	3233	141.4	2.42	48	1.89
		FF-NT3- $T_S$ + $T_S$	0.75	59.2	1727	3128	153.4	2.59	55	1.95
		FF-NT3- $T_S$ + $T_M$	0.75	69.1	1908	4718	169.4	2.45	40	1.84

## 5. Conclusions

The investigation into the progressive deformation and energy absorption characteristics of aluminum and CFRP nested-tube specimens under quasi-static lateral loading conditions has yielded significant insights. Notably, the force–displacement behavior of the aluminum and CFRP tubes demonstrated distinct material-dependent characteristics, with aluminum tubes maintaining load-bearing capacity post the initial deformation, whereas CFRP tubes exhibited rapid force escalation followed by a sudden loss of load-carrying capability due to their brittle nature. Aluminum tubes demonstrate a sequential deformation process, with the larger tube deforming first, followed by the inner tube upon contact. This progression results in smooth, stepped force curves characteristic of ductile materials, allowing for efficient energy absorption without sudden failure. Specifically, the energy absorption values for aluminum tubes were found to be 56.4 J, 55.7 J, and 51.1 J for specimens of increasing diameters, showcasing a decreasing trend with larger diameters. Comparative analysis revealed that the NT3- $T_S$ + $T_M$  sample, which included a combination of one small tube ( $T_S$ ) and one medium tube ( $T_M$ ) within a larger tube, exhibited superior energy absorption performance. Specifically, this configuration enhanced energy absorption by 19.9 J relative to the sum of the individual tubes' energy absorption up to the corresponding displacement threshold. Furthermore, this sample configuration showed a stepped force curve, indicating progressive deformation stages, which is beneficial for controlled energy dissipation during impact.

In contrast, CFRP nested samples, while demonstrating higher specific energy absorption due to their lightweight nature, experienced abrupt decreases in load-bearing capacity upon a sequence of cracking occurring on the tube wall due to reaching higher deformation levels. These cracks occur sequentially, first at the upper and lower parts of the tube, followed by the right and left sides. This significantly impacts their load-bearing capacity and results in lower energy absorption values of 22.1 J, 29.4 J, and 32.4 J for increasing diameters. The NT3- $T_S$ + $T_S$  configuration, which involved two small CFRP tubes nested within a larger tube, achieved a significant mass reduction exceeding 27%, enhancing the

specimen's overall efficiency despite a slight decrease in absorbed energy compared to aluminum nested specimens. Based on these findings, the NT3-T<sub>S</sub>+T<sub>M</sub> combination stands out as the optimal sample for maximizing energy absorption efficiency in nested tubular structures. Future studies should explore the integration of different material combinations and investigate the effects of varying tube dimensions and wall thicknesses on energy absorption characteristics. Additionally, dynamic impact tests and real-world crash simulations would provide further validation of the observed trends and enhance the practical applicability of the findings in automotive and aerospace safety design.

**Author Contributions:** Conceptualization, M.M.Y. and M.İ.Ö.; methodology, M.M.Y. and M.İ.Ö.; formal analysis, M.M.Y. and M.İ.Ö.; investigation, M.M.Y. and M.İ.Ö.; writing—original draft preparation, M.M.Y. and M.İ.Ö.; writing—review and editing, M.M.Y. and M.İ.Ö.; visualization, M.M.Y. and M.İ.Ö. All authors have read and agreed to the published version of the manuscript.

**Funding:** This research received no external funding.

**Institutional Review Board Statement:** Not applicable.

**Informed Consent Statement:** Not applicable.

**Data Availability Statement:** The original contributions presented in the study are included in the article, further inquiries can be directed to the corresponding author.

**Conflicts of Interest:** The authors declare no conflicts of interest.

## References

- Tran, T.; Hou, S.; Han, X.; Nguyen, N.; Chau, M. Theoretical prediction and crashworthiness optimization of multi-cell square tubes under oblique impact loading. *Int. J. Mech. Sci.* **2014**, *89*, 177–193. [\[CrossRef\]](#)
- Nia, A.A.; Chahardoli, S. Mechanical behavior of nested multi-tubular structures under quasi-static axial load. *Thin-Walled Struct.* **2016**, *106*, 376–389. [\[CrossRef\]](#)
- Usta, F.; Türkmen, H.S. Experimental and numerical investigation of impact behavior of nested tubes with and without honeycomb filler. *Thin-Walled Struct.* **2019**, *143*, 106256. [\[CrossRef\]](#)
- Wang, Y.; He, Q.; Li, L.; Jiang, Y. Mechanical properties of a novel nested tube and its application as anti-explosion layer. *Mater. Today Commun.* **2022**, *31*, 103242. [\[CrossRef\]](#)
- Yang, K.; Chen, Y.; Liu, S.; Qiao, C.; Yang, J. Internally nested self-locked tube system for energy absorption. *Thin-Walled Struct.* **2017**, *119*, 371–384. [\[CrossRef\]](#)
- Baroutaji, A.; Sajjia, M.; Olabi, A.-G. On the crashworthiness performance of thin-walled energy absorbers: Recent advances and future developments. *Thin-Walled Struct.* **2017**, *118*, 137–163. [\[CrossRef\]](#)
- Magliaro, J.; Altenhof, W.; Alpas, A.T. A review of advanced materials, structures and deformation modes for adaptive energy dissipation and structural crashworthiness. *Thin-Walled Struct.* **2022**, *180*, 109808. [\[CrossRef\]](#)
- Dehghanpour, S.; Safari, K.H.; Barati, F.; Attar, M.M. Comparative Analysis of Energy Absorption Capacity of Single and Nested Metal Matrix Composite Tubes Under Quasi-Static Lateral and Axial Loading. *J. Solid Mech.* **2021**, *13*, 134–143. [\[CrossRef\]](#)
- Yao, R.; Pang, T.; Zhang, B.; Fang, J.; Li, Q.; Sun, G. On the crashworthiness of thin-walled multi-cell structures and materials: State of the art and prospects. *Thin-Walled Struct.* **2023**, *189*, 110734. [\[CrossRef\]](#)
- Wang, H.; Yang, J.; Liu, H.; Sun, Y.; Xu, T.X. Internally nested circular tube system subjected to lateral impact loading. *Thin-Walled Struct.* **2015**, *91*, 72–81. [\[CrossRef\]](#)
- Xu, B.; Wang, C.; Xu, W. An efficient energy absorber based on fourfold-tube nested circular tube system. *Thin-Walled Struct.* **2019**, *137*, 143–150. [\[CrossRef\]](#)
- Wang, Y.; Zhai, X.; Liu, S.; Lu, J.; Zhou, H. Energy absorption performance of a new circular-triangular nested tube and its application as sacrificial cladding. *Thin-Walled Struct.* **2020**, *157*, 106992. [\[CrossRef\]](#)
- Ying, L.; Wang, S.; Gao, T.; Dai, M.; Hu, P.; Wang, Y. Crashworthiness analysis and optimization of multi-functional gradient foam-aluminum filled hierarchical thin-walled structures. *Thin-Walled Struct.* **2023**, *189*, 110906. [\[CrossRef\]](#)
- Al Galib, D.; Limam, A. Experimental and numerical investigation of static and dynamic axial crushing of circular aluminum tubes. *Thin-Walled Struct.* **2004**, *42*, 1103–1137. [\[CrossRef\]](#)
- Mahdi, E.-S.; El Kadi, H. Crushing behavior of laterally compressed composite elliptical tubes: Experiments and predictions using artificial neural networks. *Compos. Struct.* **2008**, *83*, 399–412. [\[CrossRef\]](#)
- Elahi, S.A.; Rouzegar, J.; Niknejad, A.; Assaee, H. Theoretical study of absorbed energy by empty and foam-filled composite tubes under lateral compression. *Thin-Walled Struct.* **2017**, *114*, 1–10. [\[CrossRef\]](#)
- Niknejad, A.; Elahi, S.A.; Liaghat, G.H. Experimental investigation on the lateral compression in the foam-filled circular tubes. *Mater. Des.* **2012**, *36*, 24–34. [\[CrossRef\]](#)



18. Ding, H.; Zhu, G.; Xiang, C.; Pei, F.; Chen, J.; Wang, Y.; Chen, Q. Excellent combination of plasticity and ultra-high strength in a low-alloy automotive steel treated by conventional continuous annealing. *Mater. Sci. Eng. A* **2020**, *791*, 139694. [\[CrossRef\]](#)
19. Adanur, Ö.; Varol, F. Investigation of the effect of friction force on the energy absorption characteristics of thin-walled structures loaded with axial impact force. *Mater. Today Commun.* **2023**, *36*, 106420. [\[CrossRef\]](#)
20. Dubey, P.P.; Rex, A.V.; Raj, A.; Paul, S.K. Influence of pre-strain on tensile response of extra deep drawing (EDD) steel under varying strain rates and crash performance. *J. Alloy. Met. Syst.* **2023**, *4*, 100036. [\[CrossRef\]](#)
21. Shabani, B.; Rad, S.G.; Alijani, A.; Darvizeh, A.; Rajabiehfar, R. Dynamic plastic behavior of single and nested rings under lateral impact. *Thin-Walled Struct.* **2021**, *160*, 107373. [\[CrossRef\]](#)
22. Olabi, A.G.; Morris, E.; Hashmi, M.S.J.; Gilchrist, M.D. Optimised design of nested circular tube energy absorbers under lateral impact loading. *Int. J. Mech. Sci.* **2008**, *50*, 104–116. [\[CrossRef\]](#)
23. Baroutaji, A.; Gilchrist, M.D.; Olabi, A.G. Quasi-static, impact and energy absorption of internally nested tubes subjected to lateral loading. *Thin-Walled Struct.* **2016**, *98*, 337–350. [\[CrossRef\]](#)
24. Kahraman, Y.; Akdikmen, O. Experimental investigation on deformation behavior and energy absorption capability of nested steel tubes under lateral loading. *Eng. Sci. Technol. Int. J.* **2021**, *24*, 579–588. [\[CrossRef\]](#)
25. Atxaga, G.; Arroyo, A.; Canflanca, B. Hot stamping of aerospace aluminium alloys: Automotive technologies for the aeronautics industry. *J. Manuf. Process.* **2022**, *81*, 817–827. [\[CrossRef\]](#)
26. Hatzigeorgiou, G.D.; Beskos, D.E. Minimum cost design of fibre-reinforced concrete-filled steel tubular columns. *J. Constr. Steel Res.* **2005**, *61*, 167–182. [\[CrossRef\]](#)
27. Wu, J.; Zhang, Y.; Li, J.; Lai, X.; Duan, N. Energy absorption characteristics of nested corrugated-elliptical tubes subjected to a lateral crushing load. *Compos. Struct.* **2022**, *297*, 115926. [\[CrossRef\]](#)
28. Yang, X.; Ma, J.; Sun, Y.; Yang, J. An internally nested circular-elliptical tube system for energy absorption. *Thin-Walled Struct.* **2019**, *139*, 281–293. [\[CrossRef\]](#)
29. Altin, M.; Acar, E.; Güler, M.A. Foam filling options for crashworthiness optimization of thin-walled multi-tubular circular columns. *Thin-Walled Struct.* **2018**, *131*, 309–323. [\[CrossRef\]](#)
30. Altin, M.; Güler, M.A.; Mert, S.K. The effect of percent foam fill ratio on the energy absorption capacity of axially compressed thin-walled multi-cell square and circular tubes. *Int. J. Mech. Sci.* **2017**, *131–132*, 368–379. [\[CrossRef\]](#)
31. Wang, S.; Zhang, M.; Pei, W.; Yu, F.; Jiang, Y. Energy-absorbing mechanism and crashworthiness performance of thin-walled tubes diagonally filled with rib-reinforced foam blocks under axial crushing. *Compos. Struct.* **2022**, *299*, 116149. [\[CrossRef\]](#)
32. Xu, B.; Wang, C.; Yuen, S.C.K. Deformation Pattern and Energy Absorption Characteristics of A Four-Tube Nested System Under Lateral and Oblique Loadings. *Lat. Am. J. Solids Struct.* **2021**, *18*, e388. [\[CrossRef\]](#)
33. Wang, Y.; Zhang, R.; Liu, S.; Zhai, X.; Zhi, X. Energy absorption behaviour of an aluminium foam-filled circular-triangular nested tube energy absorber under impact loading. *Structures* **2021**, *34*, 95–104. [\[CrossRef\]](#)
34. Zhang, W.; Xu, J. Advanced lightweight materials for Automobiles: A review. *Mater. Des.* **2022**, *221*, 110994. [\[CrossRef\]](#)
35. Fontana, M.; Araujo, A.L.; Madeira, J.F.A. Optimization of a thin-walled composite crash absorber. *Thin-Walled Struct.* **2020**, *155*, 106826. [\[CrossRef\]](#)
36. Sun, G.; Chen, D.; Zhu, G.; Li, Q. Lightweight hybrid materials and structures for energy absorption: A state-of-the-art review and outlook. *Thin-Walled Struct.* **2022**, *172*, 108760. [\[CrossRef\]](#)
37. Patel, V.; Tiwari, G.; Dumpala, R. Review of the crushing response of collapsible tubular structures. *Front. Mech. Eng.* **2020**, *15*, 438–474. [\[CrossRef\]](#)
38. Magliaro, J.; Rahimidehghan, F.; Altenhof, W.; Alpas, A.T. Superior energy dissipation mechanisms compounded within composite AA6061/H130 foam structures. *Int. J. Mech. Sci.* **2023**, *238*, 107843. [\[CrossRef\]](#)
39. Gupta, N.K.; Sekhon, G.S.; Gupta, P.K. Study of lateral compression of round metallic tubes. *Thin-Walled Struct.* **2005**, *43*, 895–922. [\[CrossRef\]](#)
40. Zhang, Z. Theoretical prediction of cross-sectional deformation of circular thin-walled tube in large elastic–plastic deformation stage under lateral compression. *Thin-Walled Struct.* **2022**, *180*, 109957. [\[CrossRef\]](#)
41. Kumar, A.P.; Nagarjun, J.; Ma, Q. Potentiality of MWCNT fillers on the lateral crashworthiness behaviour of polymer composite cylindrical tubes under quasi-static loading. *J. Ind. Text.* **2022**, *51*, 7014S–7033S. [\[CrossRef\]](#)
42. Sun, G.; Guo, X.; Li, S.; Ruan, D.; Li, Q. Comparative study on aluminum/GFRP/CFRP tubes for oblique lateral crushing. *Thin-Walled Struct.* **2020**, *152*, 106420. [\[CrossRef\]](#)
43. Wazeer, A.; Das, A.; Abeykoon, C.; Sinha, A.; Karmakar, A. Composites for electric vehicles and automotive sector: A review. *Green Energy Intell. Transp.* **2022**, *2*, 100043. [\[CrossRef\]](#)
44. Tran, T.N.; Le, D.H.; Baroutaji, A. Theoretical and numerical crush analysis of multi-stage nested aluminium alloy tubular structures under axial impact loading. *Eng. Struct.* **2019**, *182*, 39–50. [\[CrossRef\]](#)
45. Bhutada, S.; Goel, M.D. Crashworthiness parameters and their improvement using tubes as an energy absorbing structure: An overview. *Int. J. Crashworthiness* **2021**, *1–32*. [\[CrossRef\]](#)
46. Alagesan, P.K.; Dirgantara, T.; Jusuf, A.; Gladys, A.K.; Ma, Q. Comparison of the lateral crushing response of thin-walled aluminum-thermoplastic polymer composite cylindrical shells. *Mech. Adv. Mater. Struct.* **2024**. [\[CrossRef\]](#)



47. Yang, H.; Guo, X.; Wang, H.; Qu, J.; Ma, Y.; Lei, H.; Chen, H. Low-velocity impact performance of composite-aluminum tubes prepared by mesoscopic hybridization. *Compos. Struct.* **2021**, 274. [[CrossRef](#)]
48. Yang, H.; Ren, Y. On energy absorption capability and controllable failure modes of CFRP circular tube using numerical simulation. *Thin-Walled Struct.* **2024**, 205. [[CrossRef](#)]

**Disclaimer/Publisher's Note:** The statements, opinions and data contained in all publications are solely those of the individual author(s) and contributor(s) and not of MDPI and/or the editor(s). MDPI and/or the editor(s) disclaim responsibility for any injury to people or property resulting from any ideas, methods, instructions or products referred to in the content.